Geochemistry, Geophysics, Geosystems

RESEARCH ARTICLE
10.1029/2018GC007669

Time-Asymmetric FORC Diagrams: A New Protocol for Visualizing Thermal Fluctuations and Distinguishing Magnetic Mineral Mixtures

Thomas A. Berndt[1], **Liao Chang**[1,2], **Shishun Wang**[1], **and Sijibomioluwa Badejo**[3]

[1]Laboratory of Orogenic Belts and Crustal Evolution, School of Earth and Space Sciences, Peking University, Beijing, China, [2]Laboratory for Marine Geology, Qingdao National Laboratory for Marine Science and Technology, Qingdao, China, [3]Department of Earth Science and Engineering, Imperial College London, London, UK

Abstract First-order reversal curves (FORCs) are nowadays routinely used to assess domain states and magnetostatic interactions of magnetic minerals. While a huge step forward from bulk magnetic measurements in terms of sample characterization, there is a *missing link* between the FORC diagrams and remanence behavior: FORC diagrams mainly reveal domain states, while remanence behavior is largely controlled by thermal activations. We present a new tool to visualize thermal fluctuations in so-called time-asymmetric (TA) FORC diagrams. TA-FORCs differ from traditional FORCs in that they maintain the reversal field H_a for a longer time (minutes) than the FORC measurement field H_b (milliseconds). During this extended hold time, thermal activations cause some magnetic grains to change their magnetization, giving rise to an upward shift in the FORC diagram. The magnitude of this shift gives insight into the thermoviscous stability of the mineral and its remanence acquisition behavior. This not only allows to distinguish thermoviscous effects in FORC diagrams from magnetostatic (i.e., interactions/domain state related) effects but also provides a way to separate mixtures of magnetic minerals: two minerals with similar coercivity spectra that would totally overlap in traditional FORC diagrams show different upward shifts in TA-FORC diagrams, which in some cases enable complete separation of the minerals visually. This effectively provides two independent FORC signatures for two magnetic constituents in a sample such as two grain populations of different grain sizes, grain shapes, and/or mineral.

Key Points:
- We propose time-asymmetric FORC diagrams that have an extended hold time at the reversal field H_a
- Time-asymmetric FORC diagrams visualize thermal activations in FORC diagrams
- Time-asymmetric FORC diagrams enable discrimination of magnetic mineral mixtures

Supporting Information:
- Supporting Information S1

Correspondence to:
T. A. Berndt,
tberndt@pku.edu.cn

Citation:
Berndt, T. A., Chang, L., Wang, S., & Badejo, S. (2018). Time-asymmetric FORC diagrams: A new protocol for visualizing thermal fluctuations and distinguishing magnetic mineral mixtures. *Geochemistry, Geophysics, Geosystems*, *19*, 3056–3070. https://doi.org/10.1029/2018GC007669

Received 24 MAY 2018
Accepted 3 AUG 2018
Accepted article online 14 AUG 2018
Published online 10 SEP 2018

1. Introduction

First-order reversal curve (FORC) diagrams (Pike et al., 1999; Roberts et al., 2000) are nowadays routinely used to assess domain states and magnetostatic interactions of magnetic mineral assemblages. FORCs are a set of partial hysteresis loops that are measured by reducing an applied field from saturation to a reversal field H_a and then measuring a partial hysteresis loop while increasing the field H_b backup. This set of hysteresis loops is visualized as a contour plot of the mixed second derivative, the FORC diagram. FORC diagrams have been successful at characterizing domain states of samples, for example, distinguishing pseudo-single-domain (PSD) behavior from mixtures of single-domain (SD) and multidomain (MD) behavior (Muxworthy et al., 2005), magnetic mineral identification (Egli et al., 2010; Roberts et al., 2006), and at providing insights into variations of environmental magnetic records (e.g., Chang et al., 2014, 2016; Channell et al., 2016; Hatfield et al., 2017; Yamazaki, 2009), among others (see Roberts et al., 2014). In most current applications, FORC diagrams are therefore used as a tool for sample characterization, particularly in terms of domain states and magnetostatic interactions. Often, this is done qualitatively by visual inspection, but recently also quantitatively using principal component analysis (PCA) to unmix contributions of different magnetic constituents (Channell et al., 2016; Harrison et al., 2018; Lascu et al., 2015; Roberts et al., 2018).

Few works used FORC diagrams to characterize remanence behavior (Church et al., 2016; Muxworthy & Heslop, 2011; Muxworthy et al., 2011; Zhao et al., 2017). Muxworthy et al. (2011), for example, measured FORC diagrams to obtain sufficient insight into a sample's magnetic composition that thermal remanent magnetization acquisition could be modeled and paleointensities could be reconstructed without having to thermally demagnetize the sample. The fact that such little work has been done on predicting remanence behavior from FORC diagrams is most likely due to the fact that the theoretical framework of FORC diagrams is based on the simplified assumption of magnetic hysterons (termed Preisach, 1935, theory): elementary square hys-

teresis loops corresponding to the magnetic particles that switch their magnetization state only in response to the applied field and some magnetostatic interaction field. While this assumption is undoubtedly helpful for characterization of domain states, whose behavior is fundamentally determined by their magnetostatic interactions, it completely neglects the thermal fluctuation field, which is responsible for the blocking and unblocking of magnetic grains, and therefore for remanence acquisition (Néel, 1949). The model by Muxworthy and Heslop (2011), based on Stancu and Spinu (1998), attempts to include thermal fluctuations in the Preisach model, but does so only simplistically by dividing the Preisach plane into superparamagnetic (SP) and stable SD regions. A more realistic model should take the gradual (thermoviscous) relaxation of the grains into account, as predicted by Néel (1949).

Some works have attempted to extend models of FORC diagrams by thermal fluctuations (Egli, 2006; Lanci, 2003; Lanci & Kent, 2018; Pike, Roberts, & Verosub, 2001). Various features that occur in FORC diagrams could be reproduced by these models. In this paper we investigate the effect of thermal fluctuations on FORC diagrams through a numerical model and experiments, with particular focus on one feature: a vertical spread in FORC diagrams that is similar in appearance to an interaction field. Moreover, we propose a new protocol that visually separates the thermal fluctuation field and the interaction field such that the two can be distinguished from each other and be quantified. This is done through use of *time-asymmetric* (TA) FORC diagrams: FORC diagrams that are measured with an extended hold period of the reversal field H_a compared to the measuring field H_b. Finally, we will show cases where mixtures of magnetic constituents with similar domain states, interactions, and coercivity spectra that cannot be distinguished in classic FORC diagrams, but may easily be distinguished in TA-FORCs due to their constituents having different thermoviscous magnetic properties (such as grain shape, volume, and spontaneous magnetization).

2. Theory

2.1. Revision of FORC Diagrams

Before starting a discussion of thermal fluctuations in FORC diagrams, we briefly describe how FORC diagrams are measured and what they represent. FORCs are partial hysteresis loops: first, a sample is saturated in a large positive field, then the applied field is reduced to the reversal field H_a, and finally a partial hysteresis loop is measured while slowly ramping up the field from H_a back to (positive) saturation. The field at which this hysteresis loop is measured (the *measurement field*) is denoted H_b. The process is then repeated (commonly 100–200 times) for a range of reversal fields H_a. All the obtained partial hysteresis loops together can be written as $M(H_a, H_b)$. The FORC distribution $\rho(H_a, H_b)$ is defined as the mixed second derivative of M, that is,

$$\rho(H_a, H_b) = -\frac{1}{2}\frac{\partial^2 M(H_a, H_b)}{\partial H_a \partial H_b}. \tag{1}$$

Normally the FORC distribution is plotted in a rotated coordinate system $H_c = (H_b - H_a)/2$, $H_u = (H_b + H_a)/2$ as a contour plot, the FORC diagram. In this set of coordinates, noninteracting, aligned (with the field axis) SD particles all plot along the $H_u = 0$ axis, and in this case H_c corresponds to the coercivity of the particles, that is, the field that is required to switch an SD particle. The H_u coordinate can loosely be interpreted as an interaction field.

2.2. Why Thermal Fluctuations Appear in FORC Diagrams

FORC diagrams are often interpreted in terms of Preisach theory: the sample is assumed to be composed of a large number of elementary square hysteresis loops, called *hysterons* (Figure 1a). Each hysteron, roughly representing an aligned SD particle, has a given microscopic coercivity H_K. The microscopic coercivity corresponds to the energy barrier that needs to be overcome in order to make a magnetic particle switch into the opposite state, that is, in case of a SD grain, to rotate its magnetic moment into the opposite direction. Traditionally, it is assumed that all this energy is provided only by the applied field H_c in the hysteresis experiment, in which case $H_K = H_c$ and the hysteresis loop follows the thin black lines (Figure 1a). In this case, the hysteron would plot on the $H_u = 0$ axis of the FORC diagram (indicating the absence of interactions), and the H_c axis would indicate the actual microscopic coercivity.

In fact, however, thermal fluctuations provide an additional energy H_q to the system. This allows the hysteron to switch states at a reduced applied field $H_c = H_K - H_q$, following the thick red line (Figure 1a). Hence, when measuring a FORC, the hysteron would switch into the lower branch at a field H_a that is smaller than the microscopic coercivity H_K. Similarly, the hysteron will switch back into the upper branch at a field H_b that is

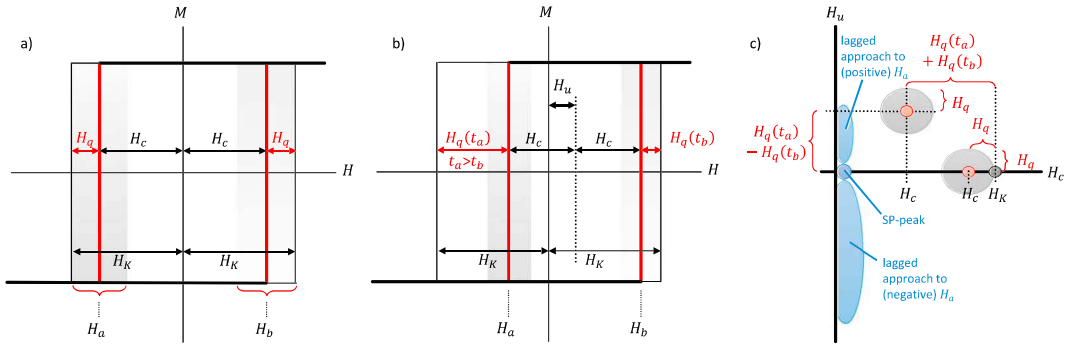

Figure 1. Schema of elementary square hysteresis loops (hysterons). Thin lines indicate hysterons as assumed by Preisach theory, thick red lines indicate the effect of a thermal fluctuation field H_q: (a) symmetric timescales imply that thermal fluctuations are equal on both sides of the loop; (b) asymmetric timescales imply that thermal fluctuations have different magnitudes on the two sides of the loop (see text for further explanations); (c) schema of thermoviscous effects of a single grain (hysteron) with microscopic coercivity H_K in a first-order reversal curve diagram: gray areas correspond to gray areas in (a) and (b), red dot correspond to red lines in (a) and (b), blue areas are explained in section 6 of the main text.

slightly smaller than H_K. As thermal fluctuations are a statistical process, not all grains switch exactly at the value, but grains switch gradually over a range of H_a and H_b, as indicated by the shaded gray area in the schema. Quantitatively, the thermal fluctuation field is given by Néel (1949) for aligned noninteracting SD particles

$$H_q(H_K, V, M_s, T, t) = \sqrt{\frac{2H_K kT \ln(t/\tau_0)}{\mu_0 V M_s}}, \tag{2}$$

where k is the Boltzmann constant, T is temperature, t is the time the field (either H_a or H_b) is applied for, τ_0 is the atomic attempt time, μ_0 is the vacuum permeability, V is the particle's volume, and M_s is the spontaneous magnetization. In the FORC diagram, a particle will therefore not plot at its microscopic coercivity on the H_c axis, but rather at a reduced value by H_q, that is, offset slightly to the left (Figure 1c). Moreover, a set of identical particles will not only plot at one value, but rather over a spread out area centering at H_K–H_q, up to a maximum of H_K. Also, because of the statistical nature of thermally activated switching, there will be a vertical spread in the FORC diagram in the H_u direction: some particles will switch at a value of H_a close to H_K but a value of H_b much below H_K, and vice versa. If $H_a \neq H_b$ then $H_u \neq 0$, such that some grains will plot above and below the $H_u = 0$ axis (Figures 1a and 1c).

2.3. Time-Asymmetric FORCs: Visualizing Thermal Fluctuations

While it is clear from the above considerations that thermal fluctuations appear in any FORC diagram in the form of a spread both along the H_u and the H_c axes, this spread is neither easily noticed visually nor easily quantifiable. We propose a new protocol that we call TA-FORCs: FORCs that are measured on asymmetric timescales, that is, a different timescale for the application of the reversal field H_a than for the measuring field H_b. The effect of asymmetric timescales on hysteresis loops is illustrated in Figure 1b: the field H_a is held for an extended time t_a (in practice, this may be of the order of 100 s). The partial hysteresis loop is then measured during a much shorter timescale, holding the measuring field H_b for some shorter time t_b (in practice, this may be a fraction of a second). From equation (2), it then follows that the thermal fluctuation field will be different in these two cases, $H_q(t_a)$ and $H_q(t_b)$, respectively. Hence, the particle will switch into the lower branch of the hysteron at a comparably small reversal field $H_a = H_K - H_q(t_a)$ but will only switch back into the upper branch at a comparably high measuring field $H_b = H_K - H_q(t_b)$. The effect of this is an apparent shift of the hysteron to the right, which manifests in the FORC diagram as an upward shift along the H_u coordinate by $H_u = (H_q(t_a) + H_q(t_b))/2$ (Figure 1c). Moreover, because of the additional (thermal) energy added into the system on the H_a side, the whole loop gets narrower; that is, H_c is further reduced compared to the above *time-symmetric* (TS) case: $H_c = H_K - H_u$.

These theoretical principles are investigated both numerically and experimentally in this study. The focus is on magnetite and titanomagnetite assemblages, the manifestation of thermal effects in their FORC diagrams and the possible use cases of TA-FORC diagrams. First, some exemplary (titano) magnetite assemblages

Table 1
Sample Characterization of Simulated and Experimental Samples

Sample	Type	V (10^{-24} m^3)	M_s (kA/m)	N	H_c (mT)	TA H_u (mT)
Magnetite	Simulation	3.4	480	0.24	20	8
TM60	Simulation	25	200	0.24	20	3–4
Elongated	Simulation	1.5	480	0.5	20	10
Rounded	Simulation	11.2	480	0.1	20	3
TC04-12-05	Experiment	~3	420	0.4	~2	5
TC04-12-06	Experiment	~4	420	0.4	~5	7
TC04-12-07	Experiment	~7	420	0.43	9	6
TC05-9.0-14	Experiment	> 7	420	0.43	55	1
Magnetite powder	Experiment	65	480	0.13	20	0

Note. V = Average grain volume; N = shape demagnetizing factor; H_c = approximate coercivity of the peak in the TS-FORC; TA H_u = approximate vertical shift in the TA-FORC. Grain sizes for Tiva Canyon samples are rough estimates from the various sources of literature given in the main text.

were numerically modeled to obtain simulated TS- and TA-FORCs, and second, well-characterized natural and synthetic samples were measured and compared to the simulations.

3. Samples

3.1. Tiva Canyon Tuff Samples

The Tiva Canyon Tuff samples are widely considered a set of natural *standard* samples due to their narrow grain size distribution of noninteracting low-Ti impure magnetite SD grains. They have been described and characterized well by many studies (e.g., Berndt et al., 2015; Berndt, Paterson, et al., 2017; Chang et al., 2014; Jackson et al., 2006; Schlinger et al., 1988; Till et al., 2011). The Tiva Canyon Tuff is a stratigraphic sequence with increasing magnetite grain sizes from the base toward the top, starting with SP grain size and ending with small PSD (i.e., vortex states) grain sizes. Grains are needle shaped, and the titanium content roughly corresponds to TM10. The samples used in this study are TC04-12-05, TC04-12-06, TC04-12-07, and TC05-9.0-14, corresponding to stratigraphic layers from about 1 m above the base to about 1.4 m above the base. TC04-12-05 has the smallest grain size and is approaching SP behavior at room temperature, TC04-12-06 and TC04-12-07 have larger grain sizes and show low-coercivity SD behavior, and TC05-9.0-14 has the largest grain sizes with higher-coercivity SD behavior, but may contain some PSD grains (i.e., vortex states). Estimates for the grain sizes of the TC04-12 samples are in the area of $3-7 \times 10^{-24}$ m^3 (see above references, Table 1).

3.2. Interacting Magnetite Powder Sample

A synthetic sample of SD magnetite powder was prepared and studied. Commercial magnetite powder by Wright Instruments, product number 4000, with a mean particle size of 50 nm was used. Yu et al. (2002) have determined the size of this powder to be 65 ± 36 nm, with an axial ratio of 1.5 ± 0.4 (corresponding to a shape anisotropy factor N of about 0.13 (Stacey & Banerjee, 1974). The same powder has been used in many other rock magnetic studies (e.g., Muxworthy et al., 2005). The powder was mixed into a polymer and compressed into a 5-mm cylindrical solid sample. No other effort than gently stirring the powder was made to disperse the magnetite grains, such that the grains are expected to strongly clump together due to their magnetostatic interactions.

3.3. Simulated Samples

In addition to experimental study, we simulated two scenarios of magnetic mineral assemblages that are likely to be representative of some natural cases of geological importance.

3.3.1. Simulated Magnetite Plus Titanomagnetite

The first scenario represents samples containing either magnetite grains, or titanomagnetite (TM60) grains, or a mixture of the two. Mixtures of magnetite and titanomagnetite are common in nature, in particular, in basalts where they form through exsolution to contain large Ti-rich grains and small Ti-poor grains (e.g., Zhou et al., 1997, 2000). Moreover, it has recently been shown that such mixtures may give rise to complex paleomagnetic behavior (Berndt, Ramalho, et al., 2017); hence, it is important to detect such mineralogies. A set of three

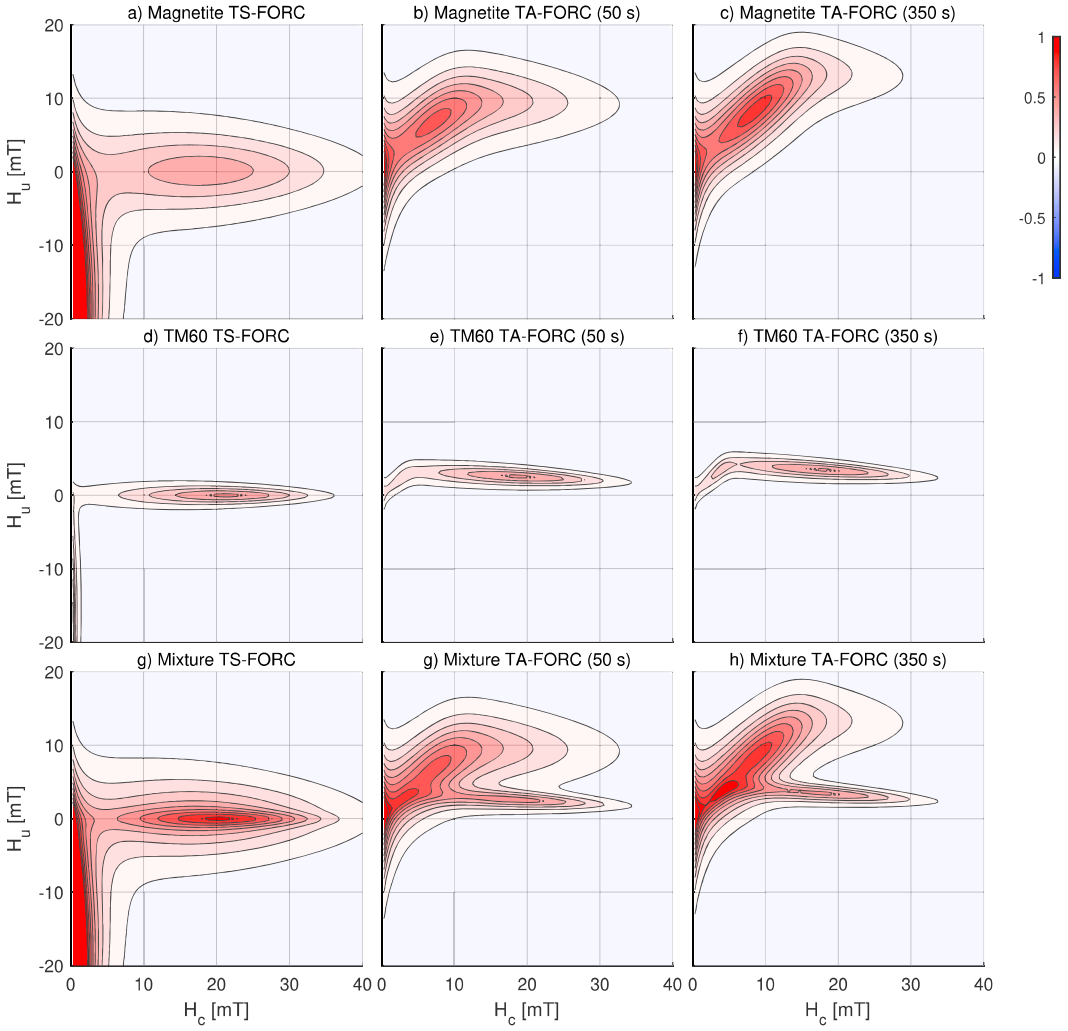

Figure 2. Simulations of TS and TA-FORC diagrams for an assembly of magnetite grains (a–c), titanomagnetite grains (d–f), and a mixture of the two (g–i). The left column shows the TS-FORC diagrams ($t_a = t_b = 125$ ms), whereas the middle and the right columns show TA-FORC diagrams with a reversal field hold time of $t_a = 50$ s and 350 s, respectively. The measuring time t_b was set to 0.125 s in all cases. All simulated FORC diagrams are unsmoothed. All plots use the same axes, color scale is normalized by the maximum peak. FORC = first-order reversal curve; TS = time-symmetric; TA = time-asymmetric.

simulations was run: (1) a pure magnetite assemblage, (2) a pure TM60 assemblage, and (3) a mixture of the two. In order to show the different thermoviscous effects of these two minerals, parameters of the two grain assemblages were chosen to have similar coercivity distributions: a lognormal distribution from SP to 40 mT, with a peak around 20 mT (Table 1 and Figure 2). The grain size distributions are shown in Figure S1 in the supporting information. Additionally, in the supporting information, simulations are shown using the same grain size distributions rather than the same coercivity distributions of the two minerals.

3.3.2. Simulated Rounded Plus Elongated Magnetite

The second modeled scenario of geological importance is the case of grain populations of the same mineral but of different shapes. This may be highly relevant in environmental magnetism, for example, when assessing contributions of different sources in a sedimentary record. Depending on the origin (e.g., biogenic and detrital), grains may be more elongated, symmetric, rounded, irregular-shaped, etc. This gives rise to different shape demagnetizing factors N, and therefore to different microscopic coercivities H_K, affecting the thermal fluctuation field in equation (2). This was tested in simulations of two populations of magnetite grains: one with a large shape demagnetizing factor, corresponding to strongly elongated needle-like grains, and one with a small shape demagnetizing factor corresponding to round, almost equant particles (Table 1). Again,

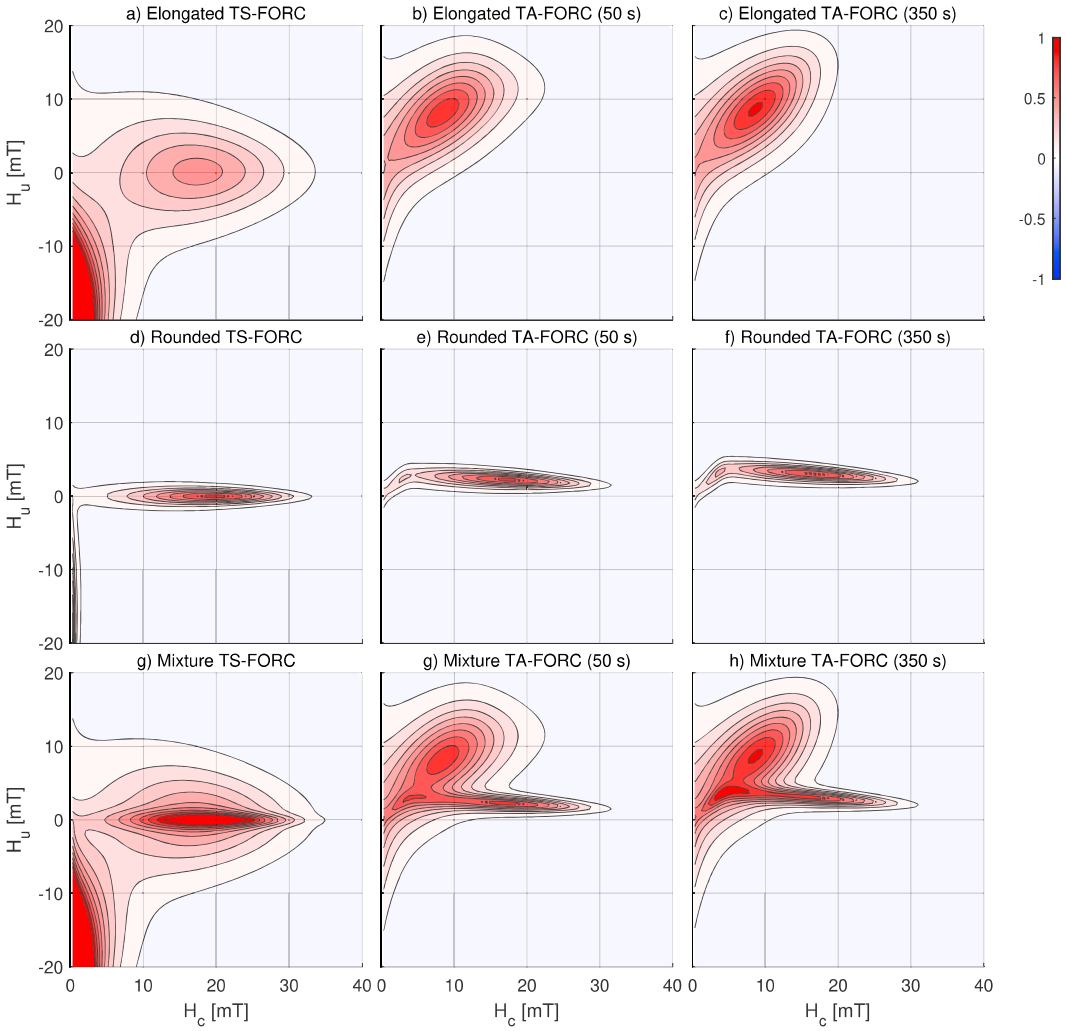

Figure 3. Simulations of time-symmetric ($t_a = t_b = 125$ ms) and time-asymmetric FORC diagrams ($t_a = 50$ s and $t_a = 350$ s, respectively) for an assembly of elongated grains with shape demagnetizing factor $N = 0.5$ (a–c), rounded grains with shape demagnetizing factor $N = 0.1$ (d–f), and a mixture of the two (g–i). All plots use the same axes; color scale is normalized by the maximum peak.

the grain size distributions were chosen such that both populations had similar coercivity spectra, peaking around 20 mT (Figures S1 and 3), but in the supporting information, additional simulations are shown using the same grain size distributions rather than the same coercivity distributions.

4. Methods

4.1. Numerical Model

Pike, Roberts, and Verosub (2001) simulated FORC diagrams including thermal fluctuations by simple forward integration of an assemblage of SD particles under application of an external field H_b that increases over small time steps $\Delta t = t_b$, starting from the reversal field H_a up to a large positive field. At each time step, H_b is slightly increased, and the thermal relaxation over the time t_b of the particles is calculated from Néel (1949) SD theory. The updated magnetization M is then calculated and the process is repeated. Recently, Lanci and Kent (2018) extended this model to account for randomly oriented Stoner and Wohlfarth (1948) particles. Here, we have reproduced the model of Pike, Roberts, and Verosub (2001) of aligned SD particles. While randomly aligned particles are more realistic, aligned particles are sufficient to produce most important features discussed above, in particular, the vertical thermal spread. We used this model to simulate TS and TA-FORCs. The only difference between the two is that thermal relaxation was calculated for an extended hold time t_a at the reversal field for the TA-FORCs. For all simulations, it was assumed that the microscopic coercivity is dom-

Table 2
FORC Settings Used to Measure Experimental TS and TA-FORCs

Sample	Tiva Canyon			Magnetite powder	
Sample type	(low-coercivity SD)			(interacting SD)	
FORC type	TS	TA	TA	TS	TA
Pause reversal t_a	125 ms	50 s	350 s	125 ms	200 s
Averaging time t_b	120 ms	120 ms	120 ms	120 ms	120 ms
H_{b1}		−20 mT		−50 mT	
H_{b2}		20 mT		50 mT	
H_{c1}		0 mT		0 mT	
H_{c2}		40 mT		100 mT	
H_{Ncr}		750 μT		1 mT	
N_{Forc}		114		207	
H_{Sat}		1 T		1 T	
Slew rate		1 T/s		1 T/s	
Pause calibration		1 s		1 s	
Pause saturation		1 s		1 s	
Smoothing factor		2–3.5		5	
Total time	0:40 hr	2:20 hr	12 hr	1:50 hr	13:20 hr

inated by shape anisotropy through the relationship $H_K = NM_s$, where N is the shape anisotropy factor. This assumption holds well for magnetite and titanomagnetite. For other minerals, for example, hematite, which are dominated by other anisotropies (e.g., magnetoelastic) this assumption does not hold (however, the conclusions would be the same as long as one chooses H_K appropriately). Magnetostatic interactions were not modeled—all the grains in the ensemble are perfectly noninteracting.

4.2. Experiments

In order to verify our theoretical predictions, a set of FORC experiments was performed. FORCs were measured on Princeton VSMs at the Institute of Rock Magnetism. The FORC measurement settings were chosen to coincide with the simulations as far as possible (Table 2), although due to time constraints some of the TA-FORC were set to only $t_a = 200$ s. The increased hold time t_a means that TA-FORCs take longer to measure than their TS counterparts; however, for modest t_a, TA-FORCs do not take excessively long (e.g., the 50-s TA-FORCs took 2:20 hr, Table 2). FORCs were measured at very high resolution, with a spacing of 750 μT of H_a fields (1 mT for the synthetic magnetite sample). Three sets of samples were measured: the first sample set consists of four Tiva Canyon Tuff samples containing noninteracting SD magnetite (with low-Ti impurity), the second was the sample of strongly interacting synthetic SD magnetite powder, and a third sample that is presented in the supporting information was a natural SD hematite sample. The experimental FORCs were smoothed using a locally weighted regression smoothing (LOESS) algorithm (Harrison & Feinberg, 2008) with smoothing factors between 2 and 3.5 for the Tiva Canyon samples and 5 to 6 for the hematite and the synthetic magnetite powder samples.

5. Results

5.1. Simulation of Magnetite and Titanomagnetite

The TS-FORCs of the magnetite and TM60 ensembles (Figure 2, left column) all show the peaks around 20 mT on the $H_u = 0$ axis, as is expected for the modeled SD grain distributions. Notably, Figure 2a shows a relatively large vertical spread of $H_u \approx \pm 5$ mT. In this case, the vertical spread is exclusively due to thermal fluctuations, and it is important not to misinterpret such a spread as being due to magnetostatic interactions (no magnetostatic interactions were included in the model; Pike, Roberts, & Verosub, 2001). In the same way, commonly observed features such as a positive signal at the origin (superparamagnetic (SP)/SD grains relaxing while the field is switched from negative to positive) and a positive signal along the $H_c = 0$ axis in the bottom half of the diagram (SD grains relaxing at the reversal field), also appear in our simulations and are already known to be caused by thermal relaxation (Pike, Roberts, & Verosub, 2001). Additionally, our TS-FORC simulations show

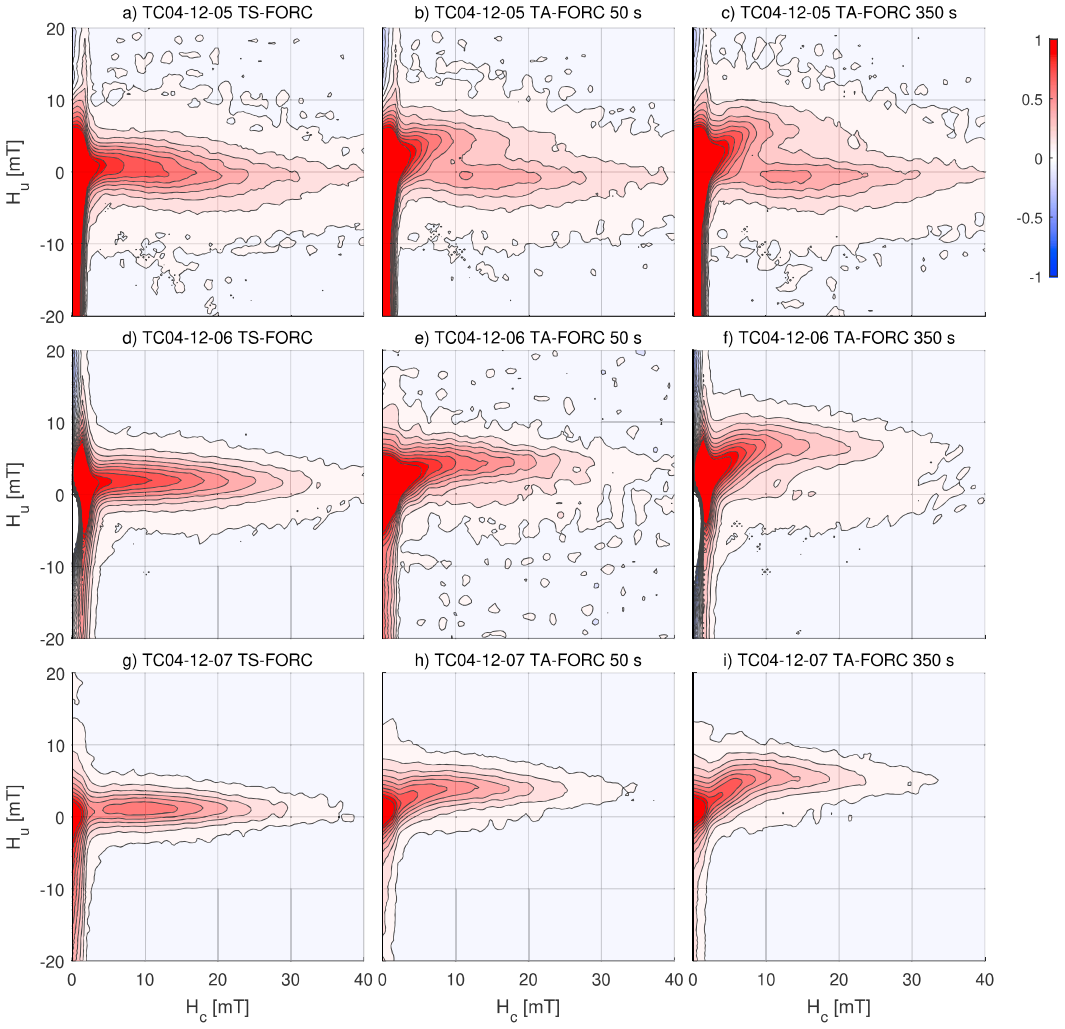

Figure 4. Experimental TS and TA-FORC diagrams for three different fine-grained Tiva Canyon samples from different stratigraphic layers with different magnetic grain sizes. Figures at the top show the finest grain size, figures at the bottom show the largest grain size. All plots use the same axes; color scale is normalized by the maximum peak.

the strong dependence of these thermal fluctuation effects on mineralogy, where the effect is much more pronounced for magnetite compared to TM60, according to the much larger V in equation (2).

The TS-FORC of the mixture of magnetite and TM60 (Figure 2g) appears very similar to the pure magnetite TS-FORC. This is because the magnetite and the TM60 peaks are almost identical, and that their FORC diagrams therefore overlap completely. The magnetite signal therefore completely swamps the TM60 signal, and it is difficult, if not impossible, to recognize the presence of the two very different minerals with very different grain sizes. The difficulty detecting such mixtures may be a problem as Berndt, Ramalho, et al. (2017) have shown that the TM60 may have an important effect on directional paleomagnetic field reconstructions. While TM60 may be detectable in $M_s(T)$ curves, this may also be difficult due to the magnetite swamping the TM60 signal with its much higher M_s.

The picture changes dramatically in TA-FORCs, which show a pronounced upward shift of the magnetite signal of up to 8 mT (middle and right columns in Figure 2 and Table 1). This upward shift is accompanied by the already known shift to lower coercivities (e.g., Lanci & Kent, 2018). The TM60 also shows an upward shift, but with much lower magnitude of only 3–4 mT. Again, the difference is due to the lower responsiveness of the large-grained TM60 to thermal fluctuations. In the simulation of the mixture this has the effect that the two minerals no longer overlap in the TA-FORCs. Rather, two distributions with separate peaks, one for magnetite at high H_u, low H_c, and one for TM60 at low H_u, high H_c, are visible. The larger the time-asymmetry (i.e., the

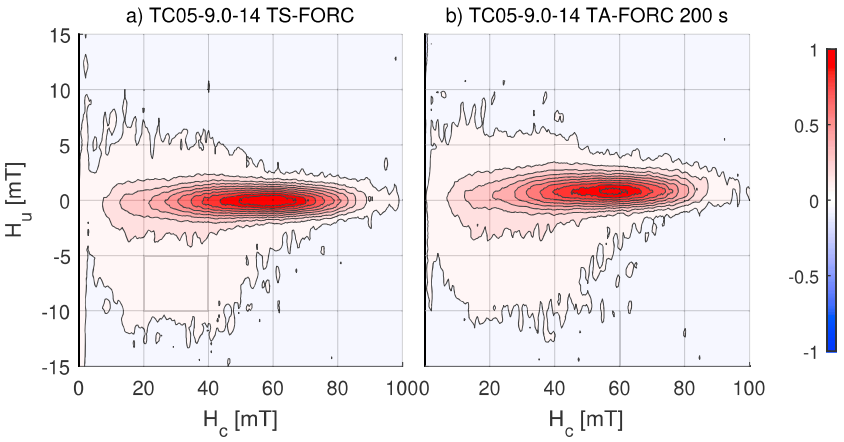

Figure 5. Experimental TS and TA-FORC diagrams for a fourth, larger-grained Tiva Canyon sample. All plots use the same axes; color scale is normalized by the maximum peak.

longer the reversal field hold time t_a), the more pronounced the separation gets, although even for a relatively slight time asymmetry, the effect is rather pronounced.

5.2. Simulation of Elongated and Rounded Grains

Also, as in the first simulation, one of the assemblages—the strongly elongated one—shows a significant amount of vertical spreading due to thermal fluctuations, whereas the other—the rounded one—shows very little. Also, the elongated grains are highly responsive to TA-FORCs, shifting upward by up to 10 mT in the 350-s diagram, while the rounded grains shift upward by only about 3 mT (Table 1). The similarities between the magnetite/TM60 grain populations and the elongated/rounded grain populations can easily be explained by equation (2): in the former case, M_s is varied, whereas in the latter case H_K is varied; H_q depends on the square root of both. Moreover, for the modeled coercivity spectrum, both the pure magnetite grain and the elongated grain distributions have smaller grain volumes than the TM60 and the rounded ensembles. As in the magnetite/TM60 case, a mixture of elongated and rounded grains (bottom row in Figure 3) produces a TS-FORC where the two populations completely overlap, whereas the two are clearly distinguishable from each other in the TA-FORCs.

5.3. Tiva Canyon Tuff Samples

Figures 4 and 5 show experimental TS- and TA-FORCs of the Tiva Canyon samples, with the smallest grain sizes at the top and the largest at the bottom. The left column shows TS-FORCs that appear as they are expected, showing increasing coercivities from top to bottom, starting from mostly SP to clear SD behavior. The TA-FORCs show a pronounced upward shift for all but the largest grain sizes of ~5–7 mT (Table 1).

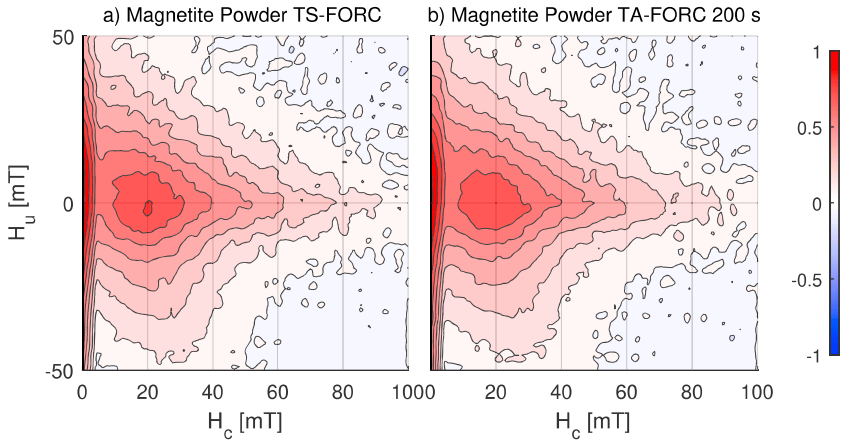

Figure 6. Experimental TS and TA-FORC diagrams for the synthetic sample of strongly interacting SD magnetite powder. All plots use the same axes; color scale is normalized by the maximum peak. Note the stretched vertical axis.

The largest grain size, TC05-9.0-14, shows an upward shift, too, but of only ~1 mT. The smaller shift is to be expected because of the larger grain volumes.

Interestingly, the smallest grained sample, TC04-12-05 very clearly shows the effect predicted for mixtures in the simulations: the TA-FORCs show two clearly discernible peaks, one showing a strong upward (and leftward) shift by 5–7 mT, and one showing no shift at all, lying on the $H_u = 0$ axis with a 10–15-mT coercivity. It may be argued that similar peaks appears in a similar location in the larger-grained samples TC04-12-06 and TC04-12-07, although less pronounced, possibly due to some overlap with the upward-shifted main peak.

5.4. Interacting Magnetite Powder Sample

Both TS- and TA-FORCs (Figure 6) show the strong magnetostatic interactions of the sample. In stark contrast to the Tiva Canyon samples, the magnetite powder shows a dispersion in H_u direction of more than 50 mT, even though the peak of the FORC distribution does not have a much higher coercivity ($H_c \approx 20$ mT). Also in stark difference to the Tiva Canyon and hematite samples, no upward shift is visible in the TA-FORC. There may be a very slight (1–2 mT) shift toward lower coercivities along the H_c axis, but this is not clearly visible due to experimental noise and smoothing.

6. Discussion

Both simulations and experiments confirm the predictions from theory: thermal fluctuations manifest themselves in TS-FORC diagrams as a vertical spread and in TA-FORC diagrams as an upward shift of the FORC distribution. This adds to a series of other, previously described thermal fluctuation effects in TS-FORC diagrams, that should be reiterated here for completeness. Afterward, the proposed new method of TA-FORCs will be discussed.

6.1. Thermal Fluctuation Effects in TS-FORCs

Thermal fluctuations in FORC diagrams were first modeled by Pike, Roberts, and Verosub (2001), who also described most of the observed effects qualitatively. The same effects were also observed and described recently by Lanci and Kent (2018) who additionally described thermal effects in randomly aligned particles.

First, and most widely known, is the SP peak at the origin of the FORC diagram (Figure 1c). The peak is due to grains that are just at the boundary between SP/SD. As they are (almost) SP, these grains align into the applied field direction (almost) immediately after changing the orientation (i.e., the sign) of the applied field. As they are close to SD, however, they do so with a slight delay, and if this delay is just of the same timescale as the instrument takes to reverse the field (from an H_a that is just below 0 to an H_b that is just above zero), it produces a signal in the FORC distribution at the origin of the diagram.

Second, a related effect is the signal along the $H_c = 0$ axis in the bottom half of the diagram, due to a time lag of grains approaching their equilibrium state for the reversal field H_a (Figure 1c). This signal occurs if the field is reduced from saturation to the reversal field H_a, and the grains at the SP/SD boundary approach the respective equilibrium state with a slight delay. Then when the field has reached H_a and is already being increased into a H_b value that is slightly above H_a (i.e., $H_u = H_b - H_a =$ small), these grains are still relaxing into the H_a equilibrium state, rather than the H_b equilibrium. At the next measurement interval, these grains have already relaxed into their H_b state and follow the field while ramping up; hence, the signal only appears very close to the vertical axis $H_c = 0$.

Third, the same effect occurs only very weakly in the top half of the FORC diagram, because the top half corresponds to positive H_a fields (Figure 1c). For negative H_a the effect is strong, because grains start at positive saturation and need to relax into an equilibrium state in the negative direction. If H_a is positive, then grains start from a positive saturation state and need to relax into the equilibrium state for a positive field, which is given by a Maxwell-Boltzmann distribution from statistical thermodynamics. The two states therefore only differ in intensity, not in sign and the signal is therefore very weak. Nevertheless, it manifests itself as a slight bending of the contour lines as they approach the $H_c = 0$ axis, and it can be seen both in the simulations and in the experimental Tiva Canyon FORCs. Even though weak, this effect can visually be a rather striking feature, especially in high-resolution FORCs at low coercivities. It is important to note that it may be quite similar to multidomain (MD) FORC signatures in appearance, even though it is completely unrelated (Pike, Roberts, Dekkers, & Verosub, 2001). The upward bending of the contour lines is a purely thermoviscous effect (Lanci & Kent, 2018). MD FORCs can, however, be distinguished, as they spread along the vertical axis in both directions equally and tend to have larger H_u than the FORC diagrams shown in this work.

Fourth, a vertical spreading is observed (gray areas in Figure 1c). This spread can be rather significant with contour lines appearing as far as 10 mT away from the $H_u = 0$ axis. The spread is due to the statistical natures of thermal relaxation: grains with a microscopic coercivity of H_K should switch at a reversal field of $H_a = H_K - H_q$, but may in fact switch anywhere close to $H_a \approx H_K - H_q$ up to $H_a > H_K$. Similarly, the same grains should switch back at $H_b = H_K - H_q$, but in fact some of them switch anywhere close to $H_b \approx H_K - H_q$ up to $H_b > H_K$. Hence, $H_u = H_b - H_a$ clusters around zero, but can be anywhere close to zero. The same type of spreading occurs in the horizontal (H_c) direction in the FORC diagram but is less obvious, as it is common for log-normally distributed grain populations to show a horizontal spreading. For the vertical spreading, however, it is important not to misinterpret it as a magnetostatic interaction field. In appearance, this vertical spread is similar to the vertical spread that is commonly observed in magnetostatically interacting grains (Figure 6). The spread here is, however, exclusively due to thermal fluctuations. Formally, the thermal fluctuation field H_q is in fact equivalent to a global interaction field H_{int}, such that in TS-FORCs the two are theoretically expected to have the same effect. Experimentally, it was observed that for very strongly interacting samples like the magnetite powder, the vertical spread can be much larger than the thermal fluctuation spread, which may potentially allow to distinguish the two in some cases.

6.2. Visualizing Thermal Fluctuations: TA-FORCs

While many of the features observed in TS-FORC diagrams are due to thermal fluctuations, as Lanci and Kent (2018) pointed out, they are hard to be analyzed, as they either manifest themselves in a similar way to other rock magnetic phenomena of interest (magnetostatic interactions, PSD, etc.), or simply reduce the observed coercivity H_c (i.e., a left-shift) and are hence indistinguishable from low H_K particles. TA-FORCs provide a direct way to resolve many of the ambiguities and to separate thermal fluctuation effects from others and to gain a much more detailed insight into a sample's magnetic composition.

Theoretical considerations as well as simulations indicate that TA-FORCs should show an upward shift of the FORC distribution. This shift is due to the increased energy provided by the thermal fluctuation field during application of the reversal field H_a. As the thermal fluctuation field is added to H_a, it actually causes a fact both in H_c and H_u direction, that is, both upward and leftward, but visually the upward motion is most obvious (Figure 1c). From equation (2) it can be seen that this shift varies with the square root of the microscopic coercivity H_K, the volume V (inversely) and the spontaneous magnetization M_s (inversely). Hence, the shift has different magnitudes for two grain populations that differ in (1) shape, or (2) grain size (i.e., volume), or (3) mineral type (i.e., M_s). The simulations have confirmed this reasoning, with grain populations of magnetite + TM60, as well as populations of elongated and rounded grains being clearly separated in TA-FORC diagrams due to their different magnitudes of the shifts.

Experimentally, the effect is confirmed by both the Tiva Canyon samples and the hematite sample (supporting information), both of which contain mostly noninteracting SD grains. The similarity, in particular, between the three finer-grained Tiva Canyon samples and the simulations for magnetite (Figure 2) are striking. Indeed, the parameters used for the simulations are roughly comparable to the Tiva Canyon samples (Table 1), although the Tiva Canyon samples contain TM10 ($M_s \approx 404$ kA/m), not pure magnetite ($M_s = 480$ kA/m). The good agreement between simulations and experiments suggest that the TA-FORC method should have the potential to quantitatively fit experimental data to simulated TA-FORC data to find best-fit values for grain size, coercivity, and spontaneous magnetization (however, it should be noted that as equation (2) depends on all three of these parameters, but FORCs are only two-dimensional, the system is still underdetermined, and only two out of the three can be uniquely determined). This compares to traditional TS-FORCs that strictly speaking determine one of these: they only estimate the coercive force H_c, which loosely relates to the microscopic coercivity H_K, neglecting the thermal fluctuation fields (which can be larger than H_K). A future quantitative analysis framework should therefore provide a wealth of additional information compared to TS-FORCs.

6.2.1. Potential of Distinguishing Grain Populations in a Single Sample

One of the most intriguing use cases of TA-FORCs may be their potential to separate FORC distributions of mixed grain/mineral populations in a single sample: while all grain populations tend to center around the $H_u = 0$ axis in TS-FORCs and therefore tend to completely overlap and possibly swamp the other signal, in

TA-FORCs, different grain populations tend to plot in different areas in H_u direction, according to their different thermal fluctuation fields H_q. In principle, the FORC signatures of two grain/mineral populations in a single sample could thus be studied independently, either qualitatively by visual inspection of the FORC diagram, or quantitatively by methods such as FORC-PCA (Channell et al., 2016; Harrison et al., 2018; Lascu et al., 2015; Roberts et al., 2018). Theoretically, it was shown that this should work for grain populations differing in grain size, grain shape, coercivity, and/or spontaneous magnetization. The ability of TA-FORCs to separate mixtures of different grain populations may be relevant for studies of paleomagnetic field reconstruction of igneous rocks that often contain mixtures of magnetite, TM, and/or other iron oxides. Vector demagnetization plots of such samples may often be misleading (Berndt, Ramalho, et al., 2017), and TA-FORCs provide a way to (1) detect such mixtures and (2) possibly quantify them.

Another use case would be the application of TA-FORCs to sedimentary samples that contain magnetic particles from different sources, which may contain biogenic magnetite, detrital magnetite, magnetite inclusions in silicate crystals (Chang et al., 2014, 2016), etc. Separating these contributions is a major challenge in current environmental magnetism. Even though significant progress has already been made, for example, by using PCA (Channell et al., 2016; Harrison et al., 2018; Heslop et al., 2014; Lascu et al., 2015), TA-FORCs potentially provide a much more direct way of separating different signals even from a single sample or might be used as additional input data for a future PCA method. Given that the different sources in sedimentary records have distinctly different grain shapes and sizes, this should be a prime use case of TA-FORCs.

6.2.2. Potential to Detect Magnetostatic Interactions

Strikingly, it has been observed that the vertical shift completely disappears in the strongly interacting SD sample 6. This may potentially be a powerful method to distinguish interacting from noninteracting SD grains: traditionally, all vertical spreading in TS-FORC diagrams is interpreted as magnetostatic interactions (if there are no PSD/MD grains; Roberts et al., 2000, 2014). This work (also, Lanci & Kent, 2001, 2018) has shown that in TS-FORCs vertical spreading can also be caused by thermal fluctuations, such that interacting and noninteracting samples are not necessarily distinguishable. Experimentally, it was found that TA-FORCs show a clear shift in addition to the spread for noninteracting particles but not for the strongly interacting sample. This could be used to uniquely resolve the ambiguity around magnetostatic interactions in FORC diagrams. From the current work it is unclear, how strong (or weak) of magnetostatic interactions are necessary to suppress the vertical shift. It is conceivable that even weak interactions of, say clusters of just a few SD grains each may be enough to suppress the shift, in which case TA-FORC would be much more sensitive for detection of weak interactions than TS-FORCs, or if only strong interactions suppress the shift. Hence, whether the suppression applies only to strongly interacting samples or also to weakly interacting samples will need to be further investigated, but in either case TA-FORCs may yield additional information about magnetostatic interactions compared to TS-FORCs. Another unanswered question is whether the strong interchain interactions of magnetosome chains created by magnetotactic bacteria affect TA-FORC diagrams: these chains are known to collectively appear like a noninteracting elongated SD signal along the central ridge in the FORC diagram (Egli et al., 2010); however, much less is known about their thermoviscous properties in FORC diagrams. It is conceivable that their thermoviscous behavior in TA-FORC diagrams provides an additional means to recognize and/or characterize magnetofossils.

6.2.3. Potential to Study Remanence Behaviour

Until recently, FORC diagrams were generally considered a tool to study domain states: SD, PSD, MD, and interacting SD samples all have their characteristic features in FORC diagrams. Much of the paleomagnetic community is, however, rather interested in remanence behavior of their samples: how do samples acquire, retain and demagnetize thermal remanent magnetizations, viscous remanent magnetizations, etc.? The questions are answered by Néel (1949) theory of thermal fluctuations of SD particles (for the lack of generally accepted theories of thermal fluctuations in PSD, MD, and interacting particles). TA-FORCs have the potential to bridge the two: they show both *domain states* (along with their characteristic properties like coercivity distribution), and the thermal fluctuations that are responsible for the *remanence behavior* of the sample (also compare; Zhao et al., 2017). As H_q depends in the same way on $\ln(t/\tau_0)$ and on the temperature T, the observations from TA-FORCs at extended timescales t_a are directly analogous to the sample's behavior at elevated temperatures T. Hence, in principle, by studying TA-FORCs, remanence behavior of a sample can be predicted. This would be a big step forward in developing methods such as nonheating paleointensity methods (e.g.,

Muxworthy & Heslop, 2011), that currently rely on model assumptions to infer a sample's behavior at elevated temperature from hysteresis experiments at room-temperatures.

6.2.4. Application to the Tiva Canyon Samples

Even though the Tiva Canyon samples are commonly considered to have a very narrow grain size distribution and uniform mineralogy, the TA-FORCs, especially for the fine-grained samples, clearly showed exactly the effect predicted theoretically for mixtures (Figure 4): two almost separate signals with different vertical shifts in the TA-FORC diagrams. The origin of the nonshifted signal is not quite clear, but several explanations are possible. One possibility is that while the samples are approximately TM10, there may be some grains with slightly higher titanium content, and some with slightly lower titanium content. Grains (or different areas of a single grain) with different titanium content are common in nature due to exsolution of the titanium. The thermal fluctuation field is rather sensitive to changes in spontaneous magnetization (i.e., titanium content) such that this might explain the two distinct signals in the Tiva Canyon TA-FORCs: one shifted (upper) peak due to lower titanium content titanomagnetite and one almost unshifted (lower) peak due to higher titanium content titanomagnetite.

Another explanation could be the presence of magnetostatic interactions. As it was found experimentally that magnetostatic interactions may completely suppress the vertical shift, it could be that while most of the grains in the samples are noninteracting, there may be some grains that do have magnetostatic interactions, for example, through clustering. These interactions might suppress the shift for these (clustering) grains, giving rise to the two separate TA-FORC peaks: one shifted peak due to the noninteracting grains and one unshifted peak due to clusters of grains. This reasoning may be more compelling than two different TM populations because of the fact the one of the peaks in the measured TA-FORCs lies almost exactly on the $H_u = 0$ axis, whereas for two TM populations, at least a weak shift would still be expected. It is possible that even weak interactions caused by small clusters of only few particles completely suppress the shift of these clustering grains. Note that independently of the question of how strong the interactions need to be to suppress the shift, it is clear that the two distinct peaks have to be due to two distinct populations of grains (i.e., one interacting, one noninteracting, or one weakly interacting, one strongly interacting)—if all the grains were experiencing the same level of interactions, then the whole FORC distribution should move (or *not* move) in the same way, rather than splitting up into two peaks.

7. Conclusions

The present work demonstrated that the wealth of information contained in FORC diagrams used is yet far from exhausted. While presently FORC diagrams are mainly used to assess domain states and interactions only, they also contain information about the thermal fluctuation fields of the sample's magnetic constituents. These provide insight into properties such as spontaneous magnetization, grain volumes, grain shapes, and microscopic coercivities of the magnetic particles. TA-FORCs provide an easy way to make this information accessible by visualizing thermal fluctuations as an upward (and leftward) shift in the FORC diagrams, as opposed to magnetostatic interactions that are symmetric around the $H_u = 0$ axis both for TS and for TA-FORCs. Measuring TA-FORCs is as easy as measuring a traditional TS-FORC and only requires changing the hold (pause) time at the reversal field. In this study, extended hold times of up to 350 s were used, but the results suggest that even moderate hold times below 50 s, possibly as low as 10–20 s may be sufficient to obtain a clearly visible shift—this would add only 0.5–1 hr of additional experimental time. The presented experiments here are in very good agreement with theoretical predictions; future quantitative frameworks may therefore be able to obtain numerical values for grain volume, shape, coercivity, etc. by numerically fitting experimental TA-FORCs to simulations or by using PCA (Channell et al., 2016; Harrison et al., 2018; Heslop et al., 2014; Lascu et al., 2015). Moreover, TA-FORCs represent a significant improvement over TS-FORCs at distinguishing noninteracting from interacting signals. Depending on the exact influence of interactions (which will need to be further studied), this may be of great use for detection and quantification of magnetosomes in sedimentary records, which are strongly interacting chains of magnetic particles. TA-FORCs extend classical TS-FORCs by another dimension—time—and therefore multiply the information accessible in FORC diagrams. Given their simplicity of measurement, they should be a useful new tool for rock magnetists and paleomagnetists.

Acknowledgments
This research was supported by a Boya Postdoc Fellwoship from Peking University and a visiting researcher fellowship by the Institute of Rock Magnetism (IRM) to T. B. The IRM is a U.S. National Multiuser Facility supported through the Instrumentation and Facilities program of the National Science Foundation, Earth Sciences Division, and by funding from the University of Minnesota. Additional funding from the National Natural Science Foundation of China (grants 41574060, 41722402), and the Laboratory for Marine Geology, Qingdao National Laboratory for Marine Science and Technology (grant MGQNLM201701) enabled completion of this work. Tiva Canyon samples and Wright Magnetite powder were kindly provided by Mike Jackson and Bruce Moskowitz from the IRM. We thank Xiang Zhao and Ioan Lascu for providing constructive review comments that improved the manuscript, and Editor Joshua Feinberg for his efficient editorial handling. All experimental data as well as the numerical model are freely available on https://github.com/thomasberndt.

References

Berndt, T., Muxworthy, A. R., & Paterson, G. A. (2015). Determining the magnetic attempt time $\tau 0$, its temperature dependence, and the grain size distribution from magnetic viscosity measurements. *Journal of Geophysical Research: Solid Earth*, *120*, 7322–7336. https://doi.org/10.1002/2015JB012283

Berndt, T., Paterson, G. A., Cao, C., & Muxworthy, A. R. (2017). Experimental test of the heating and cooling rate effect on blocking temperatures. *Geophysical Journal International*, *210*(1), 255–269. https://doi.org/10.1093/gji/ggx153

Berndt, T., Ramalho, R. S., Valdez-Grijalva, M. A., & Muxworthy, A. R. (2017). Paleomagnetic field reconstruction from mixtures of titanomagnetites. *Earth and Planetary Science Letters*, *465*, 70–81. https://doi.org/10.1016/j.epsl.2017.02.033

Chang, L., Roberts, A. P., D. Heslop, Hayashida, A., Li, J., Zhao, X., et al. (2016). Widespread occurrence of silicate-hosted magnetic mineral inclusions in marine sediments and their contribution to paleomagnetic recording. *Journal of Geophysical Research: Solid Earth*, *121*, 8415–8431. https://doi.org/10.1002/2016JB013109

Chang, L., Roberts, A. P., Winklhofer, M., Heslop, D., Dekkers, M. J., Krijgsman, W., et al. (2014). Magnetic detection and characterization of biogenic magnetic minerals: A comparison of ferromagnetic resonance and first-order reversal curve diagrams. *Journal of Geophysical Research: Solid Earth*, *119*, 6136–6158. https://doi.org/10.1002/2014JB011213

Channell, J. E., Harrison, R. J., Lascu, I., McCave, I. N., Hibbert, F. D., & Austin, W. E. N. (2016). Magnetic record of deglaciation using FORC-PCA, sortablesilt grain size, and magnetic excursion at 26 ka, from the Rockall Trough (NE Atlantic). *Geochemistry, Geophysics, Geosystems*, *17*, 1823–1841. https://doi.org/10.1002/2016GC006300

Church, N. S., Fabian, K., & McEnroe, S. A. (2016). Nonlinear Preisach maps: Detecting and characterizing separate remanent magnetic fractions in complex natural samples. *Journal of Geophysical Research: Solid Earth*, *121*, 8373–8395. https://doi.org/10.1002/2016JB013465

Egli, R. (2006). Theoretical aspects of dipolar interactions and their appearance in first-order reversal curves of thermally activated single-domain particles. *Journal of Geophysical Research*, *111*, B12S17. https://doi.org/10.1029/2006JB004567

Egli, R., Chen, A. P., Winklhofer, M., Kodama, K. P., & Horng, C.-S. (2010). Detection of noninteracting single domain particles using first-order reversal curve diagrams. *Geochemistry, Geophysics, Geosystems*, *11*. https://doi.org/10.1029/2009GC002916

Harrison, R. J., & Feinberg, J. M. (2008). FORCinel: An improved algorithm for calculating first-order reversal curve distributions using locally weighted regression smoothing. *Geochemistry, Geophysics, Geosystems*, *9*, Q05016. https://doi.org/10.1029/2008GC001987

Harrison, R. J., Muraszko, J., Heslop, D., Lascu, I., Muxworthy, A. R., & Roberts, A. P. (2018). An improved algorithm for unmixing first-order reversal curve diagrams using principal component analysis. *Geochemistry, Geophysics, Geosystems*, *19*, 1595–1610. https://doi.org/10.1029/2018GC007511

Hatfield, R. G., Stoner, J. S., Reilly, B. T., Tepley, F. J., Wheeler, B. H., & Housen, B. A. (2017). Grain size dependent magnetic discrimination of Iceland and South Greenland terrestrial sediments in the northern North Atlantic sediment record. *Earth and Planetary Science Letters*, *474*, 474–489. https://doi.org/10.1016/j.epsl.2017.06.042

Heslop, D., Roberts, A. P., & Chang, L. (2014). Characterizing magnetofossils from first-order reversal curve (FORC) central ridge signatures. *Geochemistry, Geophysics, Geosystems*, *15*, 2170–2179. https://doi.org/10.1002/2014GC005291

Jackson, M., Carter-Stiglitz, B., Egli, R., & Solheid, P. (2006). Characterizing the superparamagnetic grain distribution f(V, Hk) by thermal fluctuation tomography. *Journal of Geophysical Research*, *111*, B12S07. https://doi.org/10.1029/2006JB004514

Lanci, L. (2003). Introduction of thermal activation in forward modeling of hysteresis loops for single-domain magnetic particles and implications for the interpretation of the Day diagram. *Journal of Geophysical Research*, *108*(B3), 2142. https://doi.org/10.1029/2001JB000944

Lanci, L., & Kent, D. V. (2018). Thermally activated forward modeling of single-domain magnetic particles applied to first order reversal curves (FORC). *Journal of Geophysical Research: Solid Earth*, *123*, 1–14. https://doi.org/10.1002/2018JB015463

Lascu, I., Harrison, R. J., Li, Y., Muraszko, J., Channell, J. E., Piotrowski, A. M., & Hodell, D. A. (2015). Magnetic unmixing of first-order reversal curve diagrams using principal component analysis. *Geochemistry, Geophysics, Geosystems*, *16*, 2900–2915. https://doi.org/10.1002/2015GC005909

Muxworthy, A. R., & Heslop, D. (2011). A Preisach method for estimating absolute paleofield intensity under the constraint of using only isothermal measurements: 1. Theoretical framework. *Journal of Geophysical Research*, *116*, B04102. https://doi.org/10.1029/2010JB007843

Muxworthy, A. R., Heslop, D., Paterson, G. A., & Michalk, D. (2011). A Preisach method for estimating absolute paleofield intensity under the constraint of using only isothermal measurements: 2. Experimental testing. *Journal of Geophysical Research*, *116*, B04103. https://doi.org/10.1029/2010JB007844

Muxworthy, A. R., King, J. G., & Heslop, D. (2005). Assessing the ability of first-order reversal curve (FORC) diagrams to unravel complex magnetic signals. *Journal of Geophysical Research*, *110*, B01105. https://doi.org/10.1029/2004JB003195

Néel, L. (1949). Théorie du traînage magnétique des ferromagnétiques en grains fins avec applications aux terres cuites. *Annales de Géophysique*, *5*, 99–136. https://doi.org/10.1016/S0009-2509(00)00427-9

Pike, C. R., Roberts, A. P., Dekkers, M. J., & Verosub, K. L. (2001). An investigation of multi-domain hysteresis mechanisms using FORC diagrams. *Physics of the Earth and Planetary Interiors*, *126*(1-2), 11–25. https://doi.org/10.1016/S0031-9201(01)00241-2

Pike, C. R., Roberts, A. P., & Verosub, K. L. (1999). Characterizing interactions in fine magnetic particle systems using first order reversal curves. *Journal of Applied Physics*, *85*(9), 6660–6667. https://doi.org/10.1063/1.370176

Pike, C. R., Roberts, A. P., & Verosub, K. L. (2001). First order reversal curve diagrams and thermal relaxation effects in magnetic particles. *Geophysical Journal International*, *145*(3), 721–730. https://doi.org/10.1046/j.0956-540$\times$.2001.01419.x

Preisach, F. (1935). Über die magnetische Nachwirkung. *Zeitschrift für Physik*, *94*, 277–302. https://doi.org/10.1007/BF01349418

Roberts, A. P., Heslop, D., Zhao, X., & Pike, C. R. (2014). Understanding fine magnetic particle systems through use of first-order reversal curve diagrams. *Reviews of Geophysics*, *52*, 557–602. https://doi.org/10.1002/2014RG000462

Roberts, A. P., Liu, Q., Rowan, C. J., Chang, L., Carvallo, C., Torrent, J., & Horng, C. S. (2006). Characterization of hematite (α-Fe2O3), goethite (α-FeOOH), greigite (Fe3S4), and pyrrhotite (Fe7S8) using first-order reversal curve diagrams. *Journal of Geophysical Research*, *111*, B12S35. https://doi.org/10.1029/2006JB004715

Roberts, A. P., Pike, C. R., & Verosub, K. L. (2000). First-order reversal curve diagrams: A new tool for characterizing the magnetic properties of natural samples. *Journal of Geophysical Research*, *105*, 28,461–28,475. https://doi.org/10.1029/2000JB900326

Roberts, A. P., Zhao, X., Harrison, R. J., Heslop, D., Muxworthy, A. R., Rowan, C. J., et al. (2018). Signatures of reductive magnetic mineral diagenesis from unmixing of first-order reversal curves. *Journal of Geophysical Research: Solid Earth*, *123*, 4500–4522. https://doi.org/10.1029/2018JB015706

Schlinger, C. M., Rosenbaum, J. G., & Veblen, D. R. (1988). Fe-oxide microcrystals in welded tuff from southern Nevada: Origin of remanence carriers by precipitation in volcanic glass. *Geology*, *16*, 556–559.

Stacey, F. D., & Banerjee, S. K. (1974). *The physical principles of rock magnetism* (p. 195). Amsterdam: Elsevier.
Stancu, A., & Spinu, L. (1998). Temperature- and time-dependent Preisach model for a Stoner-Wohlfarth particle system. *Romania*, *34*(6), 3867–3875.
Stoner, E., & Wohlfarth, E. (1948). A mechanism of magnetic hysteresis in heterogeneous alloys. *Royal Society of London*, *240*(826), 599–642.
Till, J. L., Jackson, M. J., Rosenbaum, J. G., & Solheid, P. (2011). Magnetic properties in an ash flow tuff with continuous grain size variation: A natural reference for magnetic particle granulometry. *Geochemistry, Geophysics, Geosystems*, *12*, 1–10. https://doi.org/10.1029/2011GC003648
Yamazaki, T. (2009). Environmental magnetism of Pleistocene sediments in the North Pacific and Ontong-Java Plateau: Temporal variations of detrital and biogenic components. *Geochemistry, Geophysics, Geosystems*, *10*, 1–18. https://doi.org/10.1029/2009GC002413
Yu, Y., Dunlop, D. J., & Özdemir, Ã. Č (2002). Partial anhysteretic remanent magnetization in magnetite 2. Reciprocity. *Journal of Geophysical Research*, *107*(B10), 2245. https://doi.org/10.1029/2001JB001269
Zhao, X., Roberts, A. P., Heslop, D., Paterson, G. A., Li, Y., & Li, J. (2017). Magnetic domain state diagnosis using hysteresis reversal curves. *Journal of Geophysical Research: Solid Earth*, *122*, 4767–4789. https://doi.org/10.1002/2016JB013683
Zhou, W., Van der Voo, R., & Peacor, D. R. (1997). Single-domain and superparamagnetic titanomagnetite with variable Ti content in young ocean-floor basalts: No evidence for rapid alteration. *Earth and Planetary Science Letters*, *150*(3-4), 353–362. https://doi.org/10.1016/S0012-821X(97)00099-X
Zhou, W., Van der Voo, R., Peacor, D. R., & Zhang, Y. (2000). Variable Ti-content and grain size of titanomagnetite as a function of cooling rate in very young MORB. *Earth and Planetary Science Letters*, *179*(1), 9–20. https://doi.org/10.1016/S0012-821X(00)00100-X